An Improved FCS-MPC Strategy For PMSM Based On Grey Prediction And Fuzzy Dynamic Weighting Factors

Hongfei Yang*,, Tianyu Gu**, Yinghua Zhao*, Dongliang Wang***

**Branch of Qinglongsi Coal Mine, CHN Energy Yulin Energy Co, 719300, China (e-mail:747406119@qq.com).*
***College of Electrical and Control Engineering, Xi'an University of Science and Technology, 710054, China (e-mail: 128gty@163.com)*

Abstract: To optimize the performance and minimize transition times of control systems for permanent magnet synchronous motors (PMSM), this study suggests a double closed-loop finite control set model predictive control (FCS-MPC) approach. Utilizing grey prediction and fuzzy dynamic weighting factors, the strategy is designed for PMSM applications. Initially, the mathematical model of PMSM is implemented in the two-phase synchronous rotation coordinate system to introduce the double closed-loop FCS-MPC method. This includes the use of distinct model predictive controllers for the speed outer loop and current inner loop. Subsequently, the grey system is integrated into the current inner loop to precisely determine the q-axis reference current for an optimal voltage vector, enhancing resistance to interference and dynamic response capabilities. Furthermore, a fuzzy controller is incorporated to minimize transition times by dynamically adjusting weighting factors based on varying operational conditions. This strategy aims to prevent speed overshooting, reduce transition times, and enhance resistance to interference and dynamic response. The efficacy of the proposed approach is verified through simulation and experimental assessments.

Keywords: Permanent magnet synchronous motor, Finite control set model predictive control, Grey prediction, Fuzzy control.

1. INTRODUCTION

The Permanent Magnet Synchronous Motor (PMSM) has attracted considerable interest in recent times because of its impressive power density, efficiency, and dependability. It is utilized in a variety of areas such as electric vehicles, computer numerical control servo systems, wind power, and more (Li et al., 2020). Nevertheless, attaining top-notch performance in different scenarios poses a challenge for traditional control approaches. Consequently, various researchers have suggested fresh control techniques and integrated them into PMSM control systems (Liang et al., 2018).

In recent years, there has been a growing interest in the application of model predictive control (MPC) in the field of PMSM. MPC can be classified into two main types: continuous control set model predictive control (CCS-MPC) and finite control set model predictive control (FCS-MPC) (Zhang and Hou, 2018). CCS-MPC utilizes space vector pulse width modulation to generate continuous voltage vectors, while maintaining a constant switching frequency (Zhang and Hou, 2018). On the other hand, FCS-MPC outputs a limited number of voltage vectors without the need for complex space vector modulation (Yu et al., 2022). A comparison of CCS-MPC and FCS-MPC is proposed in (Yang et al., 2021). The primary distinction between CCS-MPC and FCS-MPC lies in the requirement of a modulation unit within the control system. Unlike CCS-MPC, FCS-MPC does not necessitate a modulation unit; it omits the pulse width modulation module and incorporates the inverter directly into the prediction model. By leveraging the discrete switching characteristics of the inverter, FCS-MPC utilizes a constructed voltage vector control set that allows for the direct application of the inverter's switching signal as the control action, thereby facilitating a rapid dynamic response in the drive control system. Furthermore, FCS-MPC is characterized by its straightforward and intuitive concept, enabling multivariable control and effective management of nonlinear constraints (Kouro et al., 2015; Lim et al., 2014). These notable advantages contribute to the growing interest in FCS-MPC as a subject of research. To enhance the robustness of FCS-MPC, Liu et al. (2020) proposed a predictive current control strategy to address steady-state errors resulting from parameter mismatches, albeit overlooking speed dynamic characteristics. In (Siami et al., 2018), a simplified FCS-MPC strategy is proposed to avoid a large amount of calculation, but still have speed overshoot and fluctuation. The simplification of the FCS-MPC design limits its performance in terms of switching frequency and current distortion. The influencing factors of the FCS-MPC are analyzed in (Karamanakos and Geyer, 2020), and corresponding design guidelines are provided. By introducing MPC in the speed outer loop, the overshoot can be effectively eliminated. However, the challenges associated with selecting the optimal voltage vector and the fixed cost function of FCS-MPC result in a lack of accuracy in the output switching state.

When the FCS-MPC method is employed as the control strategy for the permanent magnet synchronous motor, the control set comprises eight voltage vectors, each characterized by constant phase and amplitude. The selection of the optimal voltage vector is crucial, as it can significantly enhance the control performance of the permanent magnet synchronous motor. In (Li et al., 2024), a simplified two-step finite control set model predictive current control strategy is proposed. This strategy extends the positioning time of the reference voltage to two control periods and selects the best voltage in these two control periods Vector. (Guo et al., 2023) developed a two-stage model utilizing an offline lookup table (OLT) to identify the optimal voltage vector, thereby minimizing the number of duty cycle calculations. (Zhang et al., 2022) proposed an optimal voltage vector selection method that considers the control performance across two control periods as a unified whole. In this approach, the same voltage vector is selected as the optimal voltage vector for both control periods. In (Lee et al., 2024), the intersection point of the predicted current and the command current of the control concentrated voltage vector is first identified, after which the voltage vector at the intersection point is selected as the optimal voltage vector. Additionally, this method can reduce the total harmonic distortion (THD) of the load current. However, existing research methods primarily concentrate on utilizing the current at the present moment and the forecasted future current to identify the optimal voltage vector. These approaches do not adequately leverage historical information and overlook significant data from previous instances, leading to inefficiencies.

The selection of weighting factors is critical to the control system in FCS-MPC. Varying the weighting factors for each term in the cost function leads to differing control performance (Kusuma et al., 2021). However, the fixed weighting factors employed in current control strategies are inadequate for managing the complex and dynamic operating conditions of permanent magnet synchronous motors. Traditional approaches often depend on laborious experiments to fine-tune these weighting factors. To address this issue, numerous researchers have proposed innovative strategies that allow for the flexible adjustment of the weighting factors based on the operational conditions of the permanent magnet synchronous motor. In (Hu et al., 2023), a method for designing graph weighting factors is proposed, which determines these factors by managing the intersection area between the state boundaries of each control objective. However, for systems where all control objectives share the same priority and properties, this approach may not yield optimal results. The method described in (Liu et al., 2022) calculates the weighting factors algebraically, thereby reducing reliance on empirical adjustments, but this increases the computational burden. (Wang et al., 2022) introduced a new algorithm utilizing particle swarm optimization to modify the weighting coefficients based on the root mean square error of the steady-state current in the d and q axes, as well as the switching time. However, this method only dynamically adjusts the weighting factors of two terms in the cost function. Recently, artificial neural networks have been investigated for optimizing weighting factors in limited control set model predictive control (Vazquez et al., 2022). Nonetheless, this method has limitations in scenarios where high accuracy is essential. (Yao et al., 2024) proposed a weight factor optimization method based on an aggregated residual network (ResNet). The input layer of this proposed network incorporates the parameters and operational status of the permanent magnet synchronous motor, enabling it to predict optimal performance under varying operating conditions. However, when the parameters and operational status of the permanent magnet synchronous motor change, the network requires retraining.

Scholars have proposed various methods to address the challenges associated with the FCS-MPC strategy, including how to select the optimal voltage vector in the control set. However, these methods often overlook the utilization of historical information and fail to fully exploit historical data. Although some researchers advocate for the dynamic adjustment of weighting factors, such strategies may impose a significant computational burden and may lack adaptability to changing work environments. In order to overcome the above problems and improve the control performance of permanent magnet synchronous motor, this study presents a novel approach to double closed-loop FCS-MPC strategy utilizing grey prediction and fuzzy dynamic weighting factors. The main aim of this strategy is to enhance the performance of PMSM control systems in small to medium scale applications by minimizing switching times and increasing both dynamic and steady-state performance. The main contributions of this study are outlined below:

1. To address the issue of inadequate utilization of historical information, a gray prediction model based on FCS-MPC has been established in the current inner loop. This model effectively extracts uncertain information from historical current data to forecast future current trends, thereby yielding a more accurate optimal voltage vector. The method also improves the dynamic response and anti-interference performance of the system.
2. Fixed weight factors can increase computational burden and lack adaptability to changing working environments. To address this issue, a fuzzy controller is introduced to dynamically optimize the weight factors. The implementation of the fuzzy controller not only reduces the number of switching times but also enhances the effectiveness of control and allows for adaptation to varying working conditions. The study concludes by presenting the results of simulation and experimental analyses.

The flow chart of this study is shown in Fig. 1.

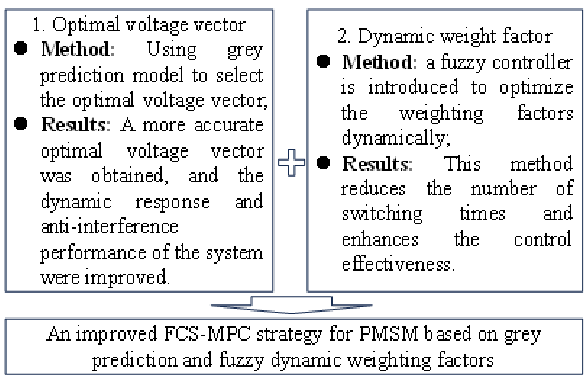

Fig. 1. The flow chart of this study.

2. SYSTEM DESCRIPTION AND FCS-MPC STRATEGY

2.1 Mathematical model of PMSM and inverter

Creating the mathematical representation of a PMSM using the theoretical model, within the d-q axis of two-phase synchronous rotation, results in the subsequent voltage equation:

$$u_{\mathrm{d}} = Ri_{\mathrm{d}} + \frac{\mathrm{d}\psi_{\mathrm{d}}}{\mathrm{d}t} - \psi_{\mathrm{q}}\omega_{\mathrm{m}} \tag{1a}$$

$$u_{\mathrm{q}} = Ri_{\mathrm{q}} + \frac{\mathrm{d}\psi_{\mathrm{q}}}{\mathrm{d}t} + \psi_{\mathrm{d}}\omega_{\mathrm{m}} \tag{1b}$$

where u_d, u_q are the d-q axis components of stator voltage, respectively; i_d, i_q are the d-q axis components of stator current, respectively; $\psi_{\mathrm{d}} = L_{\mathrm{d}}i_{\mathrm{d}} + \psi_{\mathrm{f}}$ represents the flux linkage on the d-axis, $\psi_{\mathrm{q}} = L_{\mathrm{q}}i_{\mathrm{q}}$ represents the flux linkage on the q-axis; ω_{m} denotes the electrical angular speed; ψ_{f} represents the flux linkage of the permanent magnet; R indicates the resistance of the stator; The inductances of the d-q axis are denoted as L_{d} and L_{q}. The surface-mounted PMSM discussed in this study is characterized by symmetrical d-q axis inductances, referred to as $L_{\mathrm{d}} = L_{\mathrm{q}} = L$.

The electromagnetic torque equation and the mechanical motion equation of the motor is:

$$T_{\mathrm{e}} = 1.5 p\psi_{\mathrm{f}} i_{\mathrm{q}} \tag{2}$$

$$J\frac{\mathrm{d}\omega_{\mathrm{m}}}{\mathrm{d}t} = T_{\mathrm{e}} - T_{\mathrm{L}} - B\omega_{\mathrm{m}} \tag{3}$$

where p is the number of pole pairs; J represents the moment of inertia; The electromagnetic torque and the load torque are defined as T_{e} and T_{L} respectively; B is the damping coefficient. Physical models of PMSM in three different coordinate systems are shown in Fig. 2.

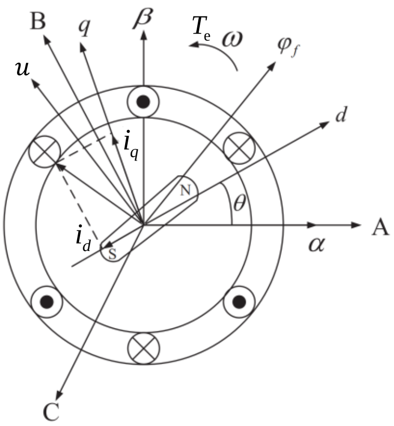

Fig. 2. Physical model of PMSM.

This paper utilizes a two-level inverter for motor drive in a three-phase system, with the schematic provided in Fig. 3. The inverter circuit is composed of six power switch tubes, including the three bridge arms, denoted as a, b and c. $S_{a,j}$, $S_{b,j}$, $S_{c,j}$, $S'_{a,j}$, $S'_{b,j}$, $S'_{c,j}$ are defined as the switching states of six power switch tubes. To avoid short circuit of direct current (DC) power supply, the power switch tubes on the same bridge arm will always be in opposite state, and "1", "0" represent open and off respectively.

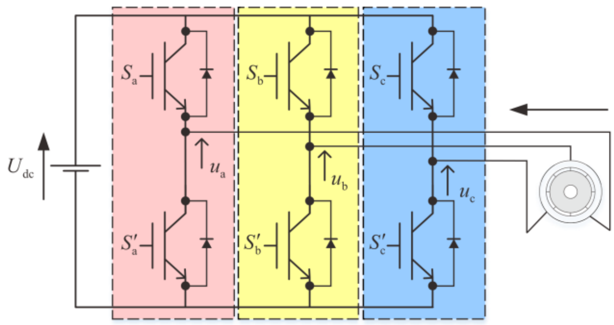

Fig. 3. Three-phase two-level inverter.

These switching signals determine the value of the output voltage:

$$u_{\mathrm{aN},j} = S_{\mathrm{a},j}U_{\mathrm{dc}} \tag{4a}$$

$$u_{\mathrm{bN},j} = S_{\mathrm{b},j}U_{\mathrm{dc}} \tag{4b}$$

$$u_{\mathrm{cN},j} = S_{\mathrm{c},j}U_{\mathrm{dc}}, \quad j = 0,1,\cdots,7, \tag{4c}$$

where $u_{\mathrm{aN},j}$, $u_{\mathrm{bN},j}$, $u_{\mathrm{cN},j}$ are the phase neutral voltages of the inverter and U_{dc} is the DC power supply voltage, $U_{\mathrm{dc}} = 220$ V.

The single vector $\mathbf{p} = e^{j2\pi/3} = -\frac{1}{2} + j\sqrt{3}/2$ shows a 120° phase difference and the output voltage vectors can be defined as:

$$\mathbf{u}_j = \frac{2}{3}(u_{\mathrm{aN},j} + \mathbf{p}u_{\mathrm{bN},j} + \mathbf{p}^2 u_{\mathrm{cN},j}), \quad j = 0,1,\cdots,7. \tag{5}$$

Considering the possible combinations of all the gated signals $S_{\mathrm{a},j}$, $S_{\mathrm{b},j}$ and $S_{\mathrm{c},j}$, eight switching states are obtained, resulting in eight voltage vectors as shown in Table 1. Fig. 4 depicts that due to $\mathbf{u}_0 = \mathbf{u}_7$, a limited collection of solely seven distinct voltage vectors can be achieved within the complex plane.

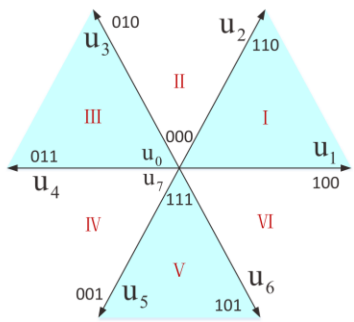

Fig. 4. Voltage vector distribution.

Table 1. Switching states of the inverter.

j	$S_{a,j}$	$S_{b,j}$	$S_{c,j}$	The voltage vector $\mathbf{u}_j$
0	0	0	0	$\mathbf{u}_0=0$
1	1	0	0	$\mathbf{u}_1=\frac{2}{3}U_{dc}$
2	1	1	0	$\mathbf{u}_2=\frac{1}{3}U_{dc}+j\frac{\sqrt{3}}{3}U_{dc}$
3	0	1	0	$\mathbf{u}_3=-\frac{1}{3}U_{dc}+j\frac{\sqrt{3}}{3}U_{dc}$
4	0	1	1	$\mathbf{u}_4=-\frac{2}{3}U_{dc}$
5	0	0	1	$\mathbf{u}_5=-\frac{1}{3}U_{dc}-j\frac{\sqrt{3}}{3}U_{dc}$
6	1	0	1	$\mathbf{u}_6=\frac{1}{3}U_{dc}-j\frac{\sqrt{3}}{3}U_{dc}$
7	1	1	1	$\mathbf{u}_7=0$

2.2 Double closed loop FCS-MPC strategy

2.2.1 Model predictive controller in speed outer loop

This study employs the model predictive control method in the speed outer loop for acquiring a higher level of precision in the q-axis reference current (Huang et al., 2021).

According to (3), the predicted speed $\omega_{pm}(k+1)$ can be expressed as:

$$\omega_{pm}(k+1)=(1-b_0)\omega_m(k)+b_0\omega_m(k-1)+a_0\Delta i_q^*(k) \tag{6}$$

where $a_0=1.5p\psi_f(1-e^{-TB/J})/B$, $b_0=-e^{-TB/J}$, $\Delta i_q^*(k)$ represents the increment of q-axis current control.

The predicted output $\omega_m(k+1)$ is:

$$\omega_m(k+1)=\omega_{pm}(k+1)+e(k), \tag{7}$$

where $e(k)=\omega_m(k)-\omega_{pm}(k)$ is the prediction error.

The reference track of speed $y_p(k+1)$ is:

$$y_p(k+1)=\tau\omega_m(k)+(1-\tau)\omega_s(k), \tag{8}$$

where τ is the flexibility coefficient, $\omega_s(k)$ is the reference speed. To minimize the deviation between the predicted output $\omega_{pm}(k+1)$ and the expected output $y_p(k+1)$ based on the reference trajectory, the secondary performance index is formulated as follows:

$$J=\lambda[\omega_{pm}(k+1)-y_p(k+1)]^2+\sigma[\Delta i_q^*(k)]^2, \tag{9}$$

where λ, σ are the degree of inhibition of tracking error and control variation, respectively. $\partial J/\partial\Delta i_q^*(k)=0$, it can be obtained as follows:

$$\begin{aligned}\Delta i_q^*(k)=&-\frac{\lambda a_0}{\lambda a_0^2+\sigma}[(1-b_0)\omega_m(k)+b_0\omega_m(k-1)\\&+e(k)-y_p(k-1)].\end{aligned} \tag{10}$$

Then, the given value of q-axis current is:

$$i_q^*(k+1)=i_q(k)+\Delta i_q^*(k). \tag{11}$$

2.2.2 FCS-MPC in current inner loop

As stated by both (1) and (3), if the motor current is chosen as the state variable, the state equation can then be derived:

$$\frac{di}{dt}=\mathrm{A}i+\mathrm{E}u+\mathrm{D}, \tag{12}$$

where $\mathrm{A}=\begin{bmatrix}-R/L & \omega_m(k)\\ -\omega_m(k) & -R/L\end{bmatrix}$, $\mathrm{E}=\begin{bmatrix}1/L & 0\\ 0 & 1/L\end{bmatrix}$,

$\mathrm{D}=\begin{bmatrix}0\\ -\psi_f\omega_m(k)/L\end{bmatrix}$, $i=\begin{bmatrix}i_d & i_q\end{bmatrix}^T$, $u=\begin{bmatrix}u_d & u_q\end{bmatrix}^T$.

If the duration of the control period T within the current inner loop is sufficiently brief, it is assumed that the input voltage u and the back electromotive force D of the system remain consistent throughout a control period $[kT,(k+1)T]$. Under these circumstances, the current forecasting model may be derived by discretizing equation (12):

$$i(k+1)=\mathrm{F}(k)i(k)+\mathrm{G}u(k)+\mathrm{M}(k), \tag{13}$$

where $i(k)=\begin{bmatrix}i_d(k) & i_q(k)\end{bmatrix}^T$, $u(k)=\begin{bmatrix}u_d(k) & u_q(k)\end{bmatrix}^T$, $\mathrm{F}(k)=\begin{bmatrix}1-TR/L & T\omega_m(k)\\ -T\omega_m(k) & 1-TR/L\end{bmatrix}$, $\mathrm{G}=\begin{bmatrix}T/L & 0\\ 0 & T/L\end{bmatrix}$, $\mathrm{M}(k)=\begin{bmatrix}0\\ -T\psi_f\omega_m(k)/L\end{bmatrix}$. Using equation (13), the stator current for each of the seven voltage vectors produced by the inverter can be accurately forecasted.

Cost function can contain multiple control objectives, variables, nonlinear conditions and other system constraints, which is the key to realizing optimal voltage vector selection. The objectives of the multi-objective cost function proposed in this paper are as follows: (1) d-axis current reference tracking; (2) q-axis current reference tracking; (3) optimization of inverter switching times; (4) restriction of current magnitude. Therefore, the cost function can be expressed as:

$$\begin{aligned}g=&Q_1 i_d^2(k+1)+Q_2(i_q^*-i_q(k+1))^2+Q_3\cdot num\\&+\hat{f}(i_d(k+1),i_q(k+1)),\end{aligned} \tag{14}$$

where $i_d(k+1)$ and $i_q(k+1)$ represent the predicted d-q axis current components corresponding to a specific voltage vector in the discrete time model of the system. The torque current reference value is denoted by i_q^*s. Q_1 and Q_2 represent the weighting factors for the d-q axis current, while Q_3 represents the weighting factor for inverter switching times. The optimal voltage vector, u_o, is established through the minimization of the cost function. In this study, the switching times for each calculation cycle in the voltage source inverter are outlined in equation (15).

$$\begin{aligned}num=&|S_a(k)-S_a(k-1)|+|S_b(k)-S_b(k-1)|\\&+|S_c(k)-S_c(k-1)|.\end{aligned} \tag{15}$$

num represents the number of switches that will occur when the voltage vector is applied to the inverter at the next moment. $S_a(k)$ and $S_a(k+1)$ denote the current and next moments, respectively, of the upper half-bridge arm switch tube of phase A of the inverter, indicating the switch status. Since both switching tubes on the same bridge arm cannot be activated simultaneously, it is sufficient to consider only the switching status of the upper half of the bridge arm.

In order to be safe, the nonlinear function of stator current limit of PMSM is designed. Its definition is shown in (16).

$$\hat{f}(i_d(k+1), i_q(k+1)) = \begin{cases} \infty, |i(k+1)| > i_{max} \\ 0, |i(k+1)| \le i_{max}. \end{cases} \qquad (16)$$

where i_{max} is the current threshold. This formula can directly eliminate the voltage vector where the current generated at the next moment exceeds the current threshold to avoid overcurrent faults.

Fig. 5 displays the block diagram of the FCS-MPC double closed-loop system for PMSM. FCS-MPC is responsible for designing the current inner loop, while the MPC algorithm is utilized for designing the speed outer loop. In summary, the algorithm known as "double closed-loop FCS-MPC" can be outlined as follows.

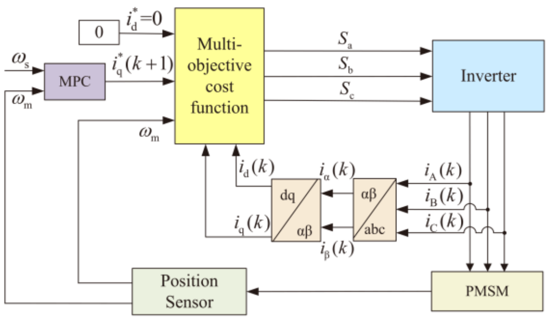

Fig. 5. Control block diagram of double closed loop FCS-MPC.

Algorithm 1

Offline stage:

1. *Choose the d-axis current* $i_d^*=0$ *and the given speed* ω_s*;*
2. *Model parameters selected are: rated voltage, number of motor pole pairs p, stator resistance R,* L_d *and* L_q *inductance for the d- and q- axis, and magnetic flux* ψ_f*.*

Online stage:

1. *Retrieve the q-axis by using the current* $i_q^*(k+1)$ *from the predictive controller of the speed outer loop model;*
2. *Substitute the reference current* i_d^*, $i_q^*(k+1)$, *actual rotational speed* $\omega_m(k)$, *d- and q- axis actual currents* $i_d(k)$ *and* $i_q(k)$ *into (13), get the current predicted value* $i(k+1)$*;*
3. *Calculate the minimum cost function through (14);*
4. *Choose the voltage vector that has the lowest cost function value, and then output the appropriate switching signal for the optimal voltage vector* u_o *to apply to the inverter in order to regulate the motor.*

In above description, as the input of current inner loop, i_q^* in next step is crucial for the selection of the optimal voltage vector. Algorithm 1 just makes use of current at present to predict i_q^* at next time, attaching less importance to current information at the past time. The accurate selection of the optimal voltage vector is hindered by this issue. Grey prediction can reveal the law of uncertain information contained in historical current data. Therefore, on the basis of Algorithm 1, grey prediction is designed to obtain more accurate optimal voltage vector.

3. DOUBLE CLOSED LOOP FCS-MPC STRATEGY BASED ON GREY PREDICTION AND FUZZY DYNAMIC WEIGHTING FACTORS

3.1 Grey prediction model

In order to improve the operational capabilities of PMSM and effectively harness ambiguous data from past current records to establish a relationship between the current value in the present and the previous output current, a grey forecasting model has been developed to predict the q-axis current and fine-tune the response mechanism.

Grey prediction can reveal the law of uncertain information contained in existing data. In the process of practical problem modeling, considering the randomness of time series data and the finiteness of data amount, it is difficult to measure the potential law of data series accurately. The process of series generation is one of the most important differences between grey prediction model and other prediction methods (Xuan et al., 2017). Grey prediction is used to model the sequence data through the unique cumulative generation transformation, which can weaken the randomness of the original data series. Using a small amount of data, it is possible for grey prediction to dig out the insignificant change trends in the original data series by accumulation transformation. Then, the grey differential equation is occupied to predict the data using accumulation generation. The grey system adopts the feedback current $i(k)$, which includes both definite and indefinite information, and generates a series of original sequences:

$$i^{(0)}(k) = \{i_1^{(0)}(k), i_2^{(0)}(k), \cdots, i_n^{(0)}(k)\}, \qquad (17)$$

where n is the extent of the sequence, and the superscript "(0)" indicates original without any accumulation. To achieve a new and unique sequence (18b), we can combine (17) into (18a).

$$i_j^{(1)}(k)=\sum_{l=1}^{j} i_l^{(0)}(k),\quad j=1,2,\cdots,n \tag{18a}$$

$$i^{(1)}(k)=\{i_1^{(1)}(k),i_2^{(1)}(k),\cdots,i_n^{(1)}(k)\}, \tag{18b}$$

where the superscript "(1)" indicates one accumulation; the subscript " j " indicates the j -th data to be predicted, with the range of values for l being 1 to j. By utilizing equation (18), the original current sequence can be reconstructed as follows:

$$i_j^{(0)}(k)=i_j^{(1)}(k)-i_{j-1}^{(1)}(k),\quad j=2,3,\cdots,n. \tag{19}$$

The definition of whitening equation is as follows:

$$i_j^{(0)}(k)+az_j^{(1)}(k)=b,\quad j=2,3,\cdots,n \tag{20}$$

$$z_j^{(1)}(k)=\frac{i_j^{(1)}(k)+i_{j-1}^{(1)}(k)}{2},\quad j=2,3,\cdots,n, \tag{21}$$

where $z^{(1)}(k)=\{z_1^{(1)}(k),z_2^{(1)}(k),\mathrm{L}\ ,z_n^{(1)}(k)\}$ is the next-mean sequence of $i^{(1)}(k)$, also known as the whitened sequence. a and b are parameters to be estimated. The whitening equation set is exhibited in (22):

$$i_2^{(0)}(k)+az_2^{(1)}(k)=b \tag{22a}$$

$$i_3^{(0)}(k)+az_3^{(1)}(k)=b \tag{22b}$$

$$\vdots$$

$$i_n^{(0)}(k)+az_n^{(1)}(k)=b. \tag{22c}$$

Through the least square method, the estimated parameters a and b can be acquired:

$$\begin{bmatrix}\hat{a} & \hat{b}\end{bmatrix}^{\mathrm{T}}=(\mathrm{Z}^{\mathrm{T}}\mathrm{Z})^{-1}\mathrm{Z}^{\mathrm{T}}\mathrm{Y}, \tag{23}$$

where $\mathrm{Z}=\begin{bmatrix}-z_2^{(1)}(k),1\\ -z_3^{(1)}(k,1\\ \cdots\cdots\\ -z_n^{(1)}(k),1\end{bmatrix}$, $\mathrm{Y}=[i_2^{(0)}(k),i_3^{(0)}(k),\cdots,i_n^{(0)}(k)]^{\mathrm{T}}$.

By solving and recovering the differential equation, the result of grey prediction is presented in the following manner:

$$\hat{i}_{j+1}^{(0)}(k+1)=(i_1^{(0)}(k)-\frac{\hat{b}}{\hat{a}})(1-e^{\hat{a}})e^{-\hat{a}k},\quad j=1,2,\cdots,n. \tag{24}$$

According to (17)-(24), current predicted at the next moment can be deduced as follows:

$$\tilde{i}_{\mathrm{q}}^{*}(k+1)=\frac{i_{\mathrm{q}}^{*}(k+1)+\hat{i}_{j+1}^{(0)}(k+1)}{2}. \tag{25}$$

The flow chart of grey prediction is shown in Fig. 6.

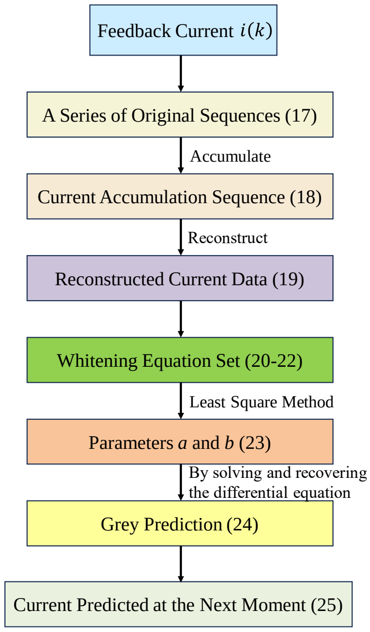

Fig. 6. Grey prediction flow chart.

Therefore, the value at the subsequent moment based on the past value is calculated, leading to an improvement in the dynamic capabilities of PMSM. The cost function is then revised to:

$$g'=Q_1 i_{\mathrm{d}}^2(k+1)+Q_2(\tilde{i}_{\mathrm{q}}^{*}-i_{\mathrm{q}}(k+1))^2+Q_3\cdot num + \hat{f}(i_{\mathrm{d}}(k+1),i_{\mathrm{q}}(k+1)). \tag{26}$$

According to the description above, the "double closed loop FCS-MPC strategy based on grey prediction" algorithm is as follows:

Algorithm 2

Offline stage:

1. *choose the d-axis current* $i_{\mathrm{d}}^{*}=0$ *and given speed* ω_{s}*;*
2. *choose the model parameters: voltage rating, number of motor pole pairs* p*, stator resistance R, inductances* L_{d} *and* L_{q} *of the d- and q- axis, and magnetic flux* ψ_{f}*.*

Online stage:

1. *the actual current* $i_{\mathrm{q}}(k)$ *of q-axis is input to the grey model equation (17)-(24), and the grey prediction current* $\tilde{i}_{\mathrm{q}}^{*}(k+1)$ *required at this moment is obtained through (25);*
2. *substitute the reference current* i_{d}^{*}, $\tilde{i}_{\mathrm{q}}^{*}(k+1)$*, actual current* $i_{\mathrm{d}}(k)$, $i_{\mathrm{q}}(k)$ *and actual rotational speed* $\omega_{\mathrm{m}}(k)$ *into (13), get the current predicted value* $i(k+1)$*;*

3. *the minimum cost function is calculated by (26);*
4. *select the voltage vector with the minimum cost function value, output the corresponding switching signal of the voltage vector u_o to be applied to the inverter in order to regulate the motor.*

Fixed weighting factors are utilized in Algorithm 1 and Algorithm 2, which require extensive experimentation to determine suitable weighting factors. These algorithms result in a significant workload and generate a large number of harmonics and switching times under different working conditions. To address this issue, a fuzzy controller can be employed to dynamically adjust the control strategy's focus and generate dynamic weighting factors, thereby avoiding the need for tedious manual adjustments. Hence, we introduce a fuzzy controller in conjunction with Algorithm 2.

3.2 Fuzzy dynamic weighting factors

In the cost function, specific weighting factors, which can adjust the emphasis ratio of different control objectives, are assigned to corresponding optimization items. In traditional methods, designers usually design a set of fixed weighting factors based on their experience. However, it is challenging for fixed weighting factors to meet both dynamic and steady-state performance requirements. Since the servo system is fundamentally a dynamic process, it proves challenging to consistently model the weighting factors for all individual terms. Therefore, this paper proposes the application of fuzzy theory for dynamically adjusting the weighting factors of multi-objective optimization. Fuzzy conditional statements and algorithms are utilized to describe the complex functional relationship between objectives. The paper presents a method for dynamically adjusting the weighting factors of the cost function, enabling optimal multi-objective assignment.

The speed deviation $\Delta\omega$ and the change rate of speed deviation $\Delta\delta$ are taken as the input variables of the fuzzy controller, where the variation range of the former is [-500, 500], and the latter is [-1000, 1000]. Weighting factors Q_1, Q_2 and Q_3 are used as output variables. The output ranges of Q_1, Q_2 and Q_3 are defined as [1, 5], [5, 9], and [0.5, 1] respectively. The input and output ranges are discretized, and fuzzy sets are defined as follows: the fuzzy sets of input variables are NB(Negative big), NM(Negative medium), NS(Negative small), ZE(Zero), PS(Positive small), PM(Positive medium), and PB(Positive big), while the fuzzy sets of output variables are ZE(Zero), PS(Positive small), PM(Positive medium), and PB(Positive big). The definition of fuzzy theory domain is shown in Table 2.

The cost function of Algorithm 1 and Algorithm 2 uses fixed weighting factors, requiring numerous experiments to be repeated for debugging based on different motors and working conditions.

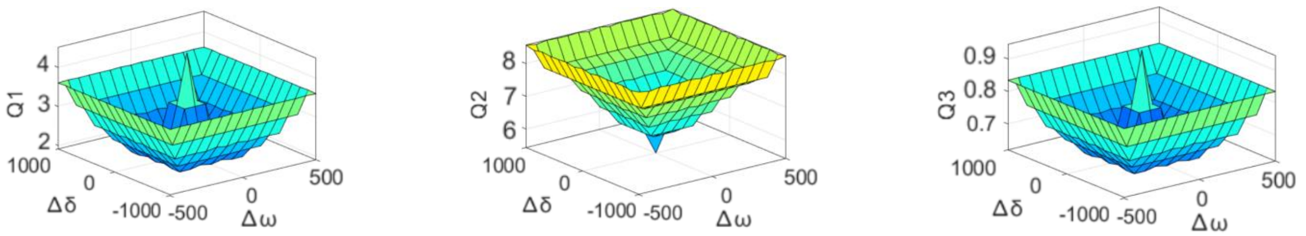

(a)Output surface of Q_1 (b)Output surface of Q_2
(c)Output surface of Q_3

Fig. 7. Input and output curves of fuzzy reasoning.

Table 2. Fuzzy theory domain.

Variables	Domain of discourse						
	NB	NM	NS	ZO	PS	PM	PB
Δω	-500	-333	-167	0	167	333	500
Δδ	-1000	-666	-333	0	333	666	1000
*Q*1	-	-	-	1	2.3	3.5	5
*Q*2	-	-	-	5	6.3	7.6	9
*Q*3	-	-	-	0.5	0.67	0.83	1

In contrast, fuzzy control does not have such limitations. By adjusting the fuzzy domain in Table 2 using a symmetrical triangle, the dynamic cost function can be achieved without the need to redesign the fuzzy rules.

Since the dynamic cost function requires real-time calculation, the shape of the membership function of the fuzzy state is a symmetric triangle, which is simple in operation, small in memory and easy in online implementation. After fuzzy reasoning rules, the center of gravity method is adopted to de fuzzy and output the fuzzy logic rules as Table 3. The input and output surfaces of fuzzy reasoning are shown in Fig.7. Fig.8 shows the control block diagram of double closed loop FCS-MPC strategy based on grey prediction and fuzzy dynamic weighting factors.

According to the above introduction of double closed loop FCS-MPC strategy based on grey prediction and fuzzy dynamic weighting factors and the structure of the control block diagram in Fig.8, the algorithm is summarized as follows:

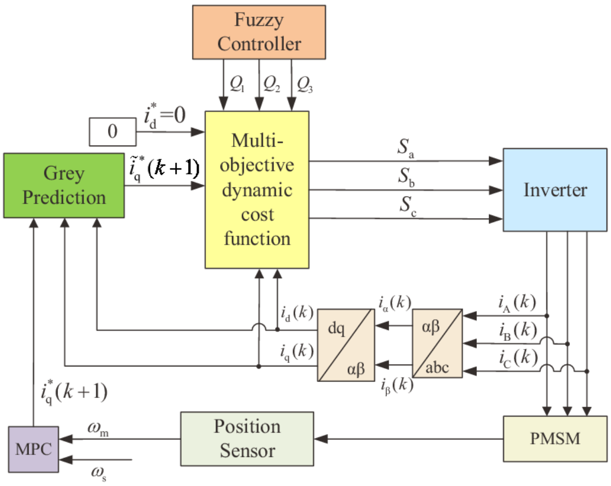

Fig. 8. Control block diagram of double closed loop FCS-MPC strategy based on grey prediction and fuzzy dynamic weighting factors.

Algorithm 3

Offline stage:

1. *choose the d-axis current* $i_d^* = 0$ *and given speed* ω_s*;*
2. *choose the model parameters: voltage rating, number of motor pole pairs* p*, stator resistance R, inductances* L_d *and* L_q *of the d- and q- axis, and magnetic flux* ψ_f*.*

Online stage:

1. *Retrieve the q-axis by using the current* $i_q^*(k+1)$ *from the predictive controller of the speed outer loop model;*
2. *the actual current* $i_q(k)$ *is input to the grey model equation (17)-(24), and the grey prediction current* $\tilde{i}_q^*(k+1)$ *required at this moment is obtained through (25);*
3. *substitute the reference current* i_d^**,* $\tilde{i}_q^*(k+1)$*, actual current* $i_d(k)$*,* $i_q(k)$ *and actual rotational speed* $\omega_m(k)$ *into (13), get the current predicted value* $i(k+1)$*;*
4. *the dynamic weighting factors* Q_1*,* Q_2 *and* Q_3 *are obtained from the fuzzy controller.*
5. *the minimum cost function is calculated by (26);*
6. *Choose the voltage vector* u_o *that has the lowest cost function value, and then produce the associated switching signal for the voltage vector in order to regulate the motor through the inverter.*

4. SIMULATION AND EXPERIMENT

4.1 Simulation results and analysis

A MATLAB/Simulink simulation model is created to evaluate three different algorithms using the control block diagrams displayed in Fig.5 and Fig.8. Evaluations were performed to analyze the efficiency of the control strategies in two scenarios: initiating operation with no load and with sudden loading. The duration of each simulation is limited to 0.4 seconds, and the necessary parameters are detailed in Table 4. The grey prediction model is able to reveal the law of the original sequence with only a small amount of data. In this paper, the original sequence length for grey prediction is selected as $n = 4$ in both simulation and experiment. Additionally, the initial value is set as 0 to reduce the computational load. After three control periods, the initial value is cleared and the system enters the normal operation state. Compared with the overall operating time, the duration of three periods is very short, and its impact on control effectiveness can be ignored.

In the control system of PMSM, it is evident from equations (2) and (3) that the current inner loop plays a crucial role in ensuring the motor torque control performance(Wang et al., 2020). The torque and speed are closely related, as the torque and load collectively determine the motor speed. Consequently, enhancing the current inner loop directly affects the evaluation of speed outcomes. Hence, this paper selects speed and current as the measurement indices.

The stated motor speed is specified at 500 revolutions per minute. Fig. 9 illustrates the speed comparison of the three tactics. It is evident from the graph that Algorithms 1 through 3 are able to reach the desired speed without experiencing any overshoot. Both Algorithm 2 and Algorithm 3 have shorter response time than Algorithm 1. When $t = 0.2$ s, a load disturbance of 2.4 $\mathrm{N \cdot m}$ was added suddenly, the speed decreased in all three strategies, but it is evident that the three algorithms successfully mitigated the speed variation resulting from changes in the load. In the steady state stage, Algorithm 3 has the smallest velocity fluctuation.

The specific index comparison results are shown in Table 5. In the motor startup stage, the rising time of Algorithm 2 and 3 are reduced by 51.34% and 58.92% respectively in comparison with Algorithm 1. Algorithm 3 can reach the steady-state in the shortest time among the three strategies. The speed fluctuation and recovery time of Algorithm 3 is the minimum under sudden load. These specific data indicate the role of grey prediction in fast dynamic response. Compared with Algorithm 1, the switching times of Algorithm 2 and 3 are reduced by 9.14% and 57.71% respectively. Meanwhile, the total harmonic distortion (THD) of A-phase current of algorithm 2 and algorithm 3 is 16.23% and 15.89% respectively, both lower than the 23.85% of algorithm 1. It can be seen that compared with Algorithm 1, Algorithm 2 improves the dynamic and anti-interference performance of the system, and also reduces switching times and THD of A- phase current. This is due to the introduction of grey prediction, which can reveal the law of uncertain information contained in historical current data to obtain the optimized q-axis reference current. With the precise reference current of q-axis from grey prediction, more accurate voltage vectors can be selected, resulting in faster dynamic response performance and fewer switching times of inverter. However, among the three strategies, Algorithm 3 has the least switching times of the inverter and the minimum THD of A-phase current in the whole control system. This is owing to the weighting factor of each term is dynamically adjusted by fuzzy controller in Algorithm 3.

Table 3. Fuzzy logic rules.

The change rate of speed deviation	Speed deviation						
	NB	NM	NS	ZO	PS	PM	PB
NB	PS,PB,PS	PS,PB,PS	PS,PB,PS	PS,PB,PS	PS,PB,PS	PS,PB,PS	PS,PB,PS
NM	PS,PB,PS	PM,PM,PM	PM,PM,PM	PM,PM,PM	PM,PM,PM	PM,PM,PM	PS,PB,PS
NS	PS,PB,PS	PM,PM,PM	PB,PS,PB	PB,PS,PB	PB,PS,PB	PM,PM,PM	PS,PB,PS
ZO	PS,PB,PS	PM,PM,PM	PB,PS,PB	ZO,ZO,ZO	PB,PS,PB	PM,PM,PM	PS,PB,PS
PS	PS,PB,PS	PM,PM,PM	PB,PS,PB	PB,PS,PB	PB,PS,PB	PM,PM,PM	PS,PB,PS
PM	PS,PB,PS	PM,PM,PM	PM,PM,PM	PM,PM,PM	PM,PM,PM	PM,PM,PM	PS,PB,PS
PB	PS,PB,PS	PS,PB,PS	PS,PB,PS	PS,PB,PS	PS,PB,PS	PS,PB,PS	PS,PB,PS

There are some schemes that dynamically adjust the weighting factors in recent literature, among which the simulated annealing algorithm proposed in (Davari et al., 2021) performs relatively well. In order to validate the efficacy of the fuzzy controller introduced in this study, the simulated annealing algorithm is compared with Algorithm 3. From the simulation results of speed waveform comparison, it can be seen that the dynamic response performance of "Algorithm proposed in (Davari et al., 2021)" is similar to that of Algorithm 3, but slightly worse than Algorithm 3 in general. The speed fluctuation of "Algorithm proposed in (Davari et al., 2021)" increases obviously, which is not conducive to the actual motor control. Therefore, Algorithm 3 has obvious advantages.

Table 4. Simulation and experiment parameters.

Parameter	Value	Parameter	Value
ω_s	500r/min	U_e	220 V
p	4	R	1.8 Ω
L_d, L_q	4.16 mH	ψ_f	0.1337 Wb
T	0.0001 s	P_e	0.6 kW

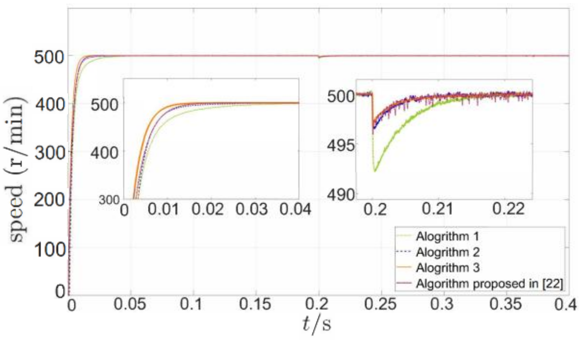

Fig. 9. The simulation results of speed waveform comparison.

Through the above analysis, it can be seen that the grey prediction in Algorithm 2 can shorten the system speed rising time and recovery time. Fuzzy controller adopted in Algorithm 3 can greatly decrease the switching times while further enhancing the superior performance of Algorithm 2.

4.2 Experimental results and analysis

Based on the theoretical introduction and simulation results, this paper builds an experimental platform of FCS-MPC system for PMSM. The control methods are implemented using a TMS320F28335. The three strategies are compared in experiments to analyze the motor response speed when starting with no load, and the anti-interference ability after the sudden loading. Motor parameters are shown in Table 4. The experimental platform is shown in Fig. 10.

The comparison of speed waveforms when starting the motor without load is shown in Fig. 11. Algorithm 2 and Algorithm 3, compared to Algorithm 1, effectively enhance dynamic response performance and reduce switching times. After the motor runs smoothly, the magnetic powder brake is used to increase the load torque, and all the three strategies will have speed fluctuation. Experimental results demonstrate that Algorithm 3 exhibits smaller speed fluctuations when the load is abruptly added, indicating superior anti-interference performance compared to the other two strategies. Additionally, Algorithm 3 shows the least speed fluctuation when the motor speed reaches the reference value, further validating the effectiveness of the algorithm in steady state.

The index comparison results are shown in Table 6. It can be observed that Algorithm 3 demonstrates the fastest speed tracking performance among the three strategies. Additionally, Algorithm 2 confirms the effectiveness of grey prediction in improving dynamic and anti-interference performance. The switching times of Algorithm 2 and 3 are reduced by 8.77% and 26.97% respectively compared to Algorithm 1. Furthermore, Algorithm 3 provides evidence of the effectiveness of a fuzzy controller in reducing the switching times of the inverter.

Table 5. Comparison of three control strategies in simulation.

Indicator	Algorithm 1	Algorithm 2	Algorithm 3	Algorithm proposed in (Davari et al., 2021)
Speed response time t_r (s)	0.0409	0.0199	0.0168	0.0187
Maximum speed fluctuation $\Delta\omega_{max}$ (r/min)	7.665	4.216	3.981	4.861
Speed recovery time t_c (s)	0.020	0.0114	0.0092	0.0102
Switching times *num*	3138	2851	1327	1563
The THD of A-phase current	23.85%	16.23%	15.89%	16.81%

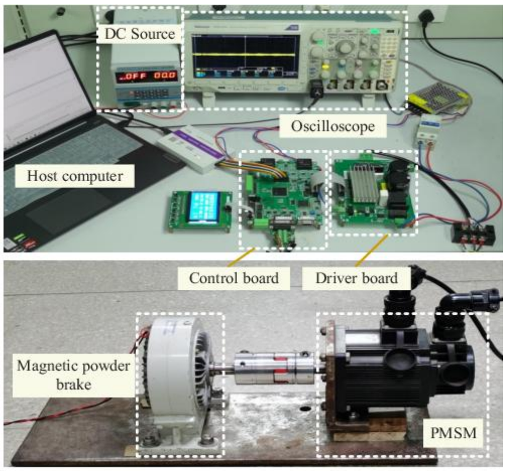

Fig. 10. The experimental platform of FCS-MPC system.

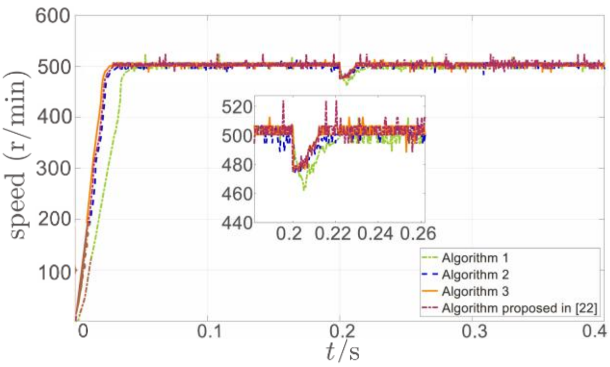

Fig. 11. The experiment results of speed waveform comparison.

Fig. 12 displays the wave patterns of the metrics. Table 6 outlines the THD of A-phase current and the fluctuations in current for the d- and q-axes. Based on the data, the following deductions can be made: (1) After sudden loading, the q-axis current of the three strategies can quickly reach the new stable value. The current responses of Algorithm 3 are better, and the q-axis current ripple of Algorithm 3 is the smallest in the three strategies. (2) The A-phase current waveforms of Algorithm 2 and Algorithm 3 exhibit lower harmoniccontent, better sinusoidal quality, and improved current response. The THD values of Algorithm 2 and Algorithm 3 are reduced by 10.88% and 12.27%, respectively, compared to Algorithm 1. (3) The d-axis current of Algorithm 3 is more stable, and the performance is better following the reference d-axis current, that is, $i_d^* = 0$.

Based on the data from the algorithm proposed in (Davari et al., 2021) in Table 6, it is evident that the speed response performance of the algorithm is comparable to that of Algorithm 3. However, it is observed that the current ripple of d-q axes and the THD value of A-phase current of the algorithm proposed in (Davari et al., 2021) increase significantly when compared to Algorithm 3. This increase in ripple and THD value will inevitably lead to a decline in the overall control performance. The effectiveness of fuzzy control in dynamically adjusting the weighting factors of the cost function is proven to offer superior performance.

The feasibility of Algorithm 2 and Algorithm 3 has been verified through experiments. The double closed loop FCS-MPC strategy, which is based on grey prediction, can improve the system's dynamic response and anti-interference performance. The double closed loop FCS-MPC strategy based on grey prediction and fuzzy dynamic weighting factors can drastically reduce the switching times and THD value of A-phase current while further improving the control performance.

Table 6. Comparison of three control strategies in experiment.

Indicator	Algorithm 1	Algorithm 2	Algorithm 3	Algorithm proposed in (Davari et al., 2021)
Speed response time *tr* (s)	0.055	0.039	0.024	0.035
Maximum speed fluctuation Δωmax (r/min)	36.362	30.512	28.438	30.917
Speed recovery time *tc* (s)	0.029	0.023	0.014	0.016
Switching times *num*	3671	3349	2681	2945
The THD of A-phase Current	32.45%	28.92%	28.47%	30.71%
Current ripple of d-axis (A)	0.0581	0.0552	0.0527	0.0638
Current ripple of q-axis (A)	0.0843	0.0821	0.0792	0.0913
Algorithm execution time (*us*)	49.21	53.86	59.34	57.81

To evaluate the robustness of Algorithm 3 under parameter mismatch, experiments were conducted to test the control performance of Algorithm 3 under resistance and inductance mismatch with no load. Fig. 13 illustrates the current waveform of 0.2~0.3s in the case of parameter mismatch of Algorithm 3. In this scenario, the d-axis current remains stable near 0, the q-axis current remains stable, and the sinusoidal degree of A-phase current remains good. These experimental results demonstrate that Algorithm 3 exhibits good robustness under parameter mismatch. Additionally, Fig. 14 displays the waveform of the weighting factors in Algorithm 3. It is evident that the fuzzy controller can dynamically adjust the weighting factors of the cost function and utilize optimized weighting factors in different running stages to achieve superior dynamic performance.

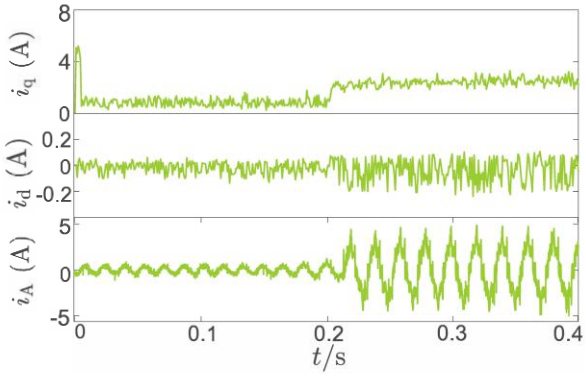

(a) Algorithm 1

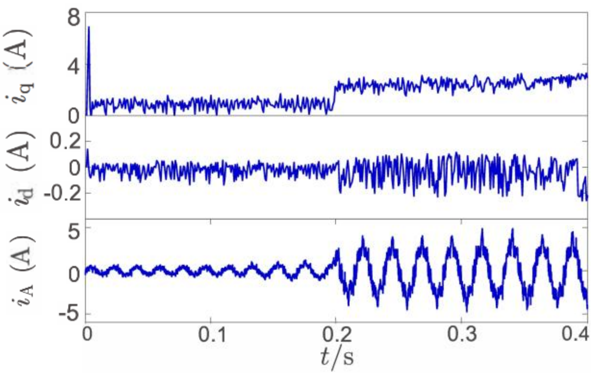

(b) Algorithm 2

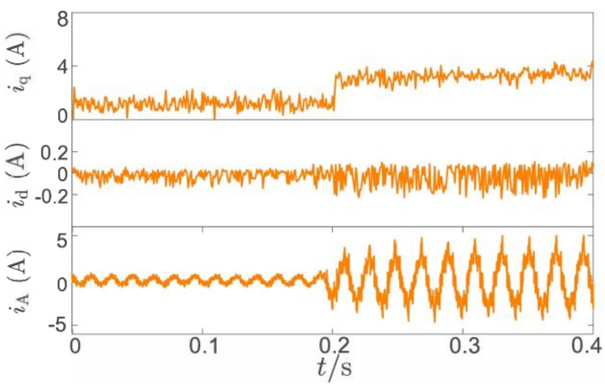

(c) Algorithm 3

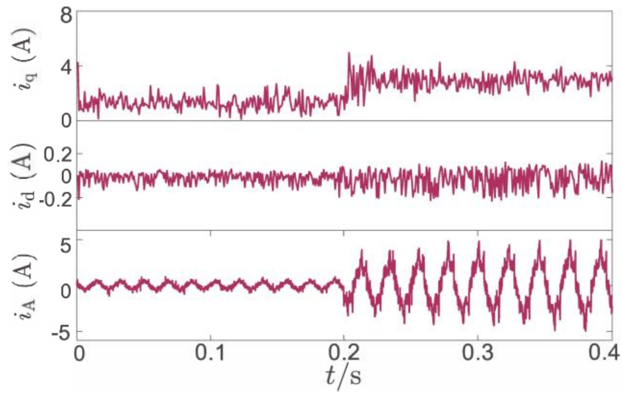

(d) Algorithm proposed in (Davari et al., 2021)

Fig. 12. The experimental results under load torque change.

To compare the computational burden of the three strategies, the execution times are shown in Table 6. It can be observed that Algorithm 1 has a lower computational burden compared to Algorithm 2 and Algorithm 3. Although the grey prediction and fuzzy dynamic weighting factors slightly increase the computational burden, the execution times do not exceed the control period, and the calculations can be completed without the need for hardware improvement.

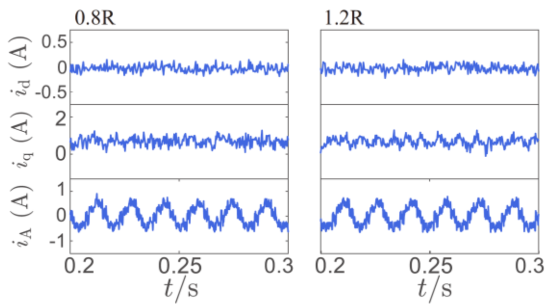

(a) Resistance mismatch

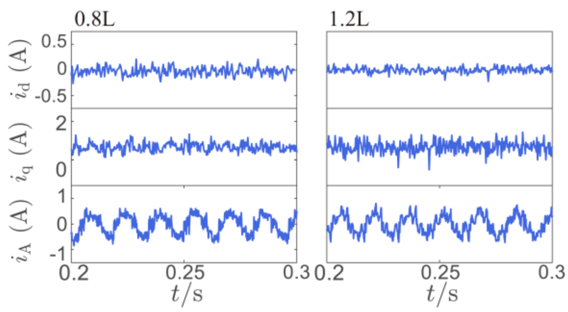

(b) Inductance mismatch

Fig. 13. The experimental waveform comparison under parameter mismatch in Algorithm 3.

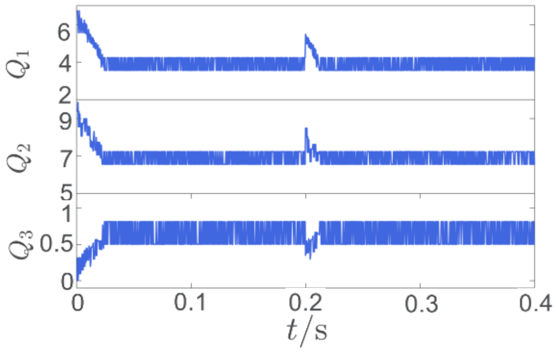

Fig. 14. Waveforms of weighting factors in Algorithm3.

By comparing Table 5 and Table 6, slight differences can be observed between the simulation and experimental results. This can be attributed to the fact that the simulation model is established under ideal conditions, whereas actual experiments are subject to various unavoidable factors such as inaccurate motor parameters, temperature changes, and unstable power quality. These factors contribute to the deviation between simulation and experimental results. However, it is noteworthy that the overall trend of the corresponding index data changes remains consistent, thereby validating the applicability of the control algorithm in practical scenarios.

5. CONCLUSIONS

To enhance the dynamic performance and anti-interference capabilities of the PMSM control system, this paper introduces a dual closed-loop strategy for FCS-MPC that utilizes grey prediction and fuzzy dynamic weighting factors. We introduce the grey prediction and fuzzy control theory to compare and analyze three strategies. Through simulation and experimental results, we have confirmed the efficacy and superiority of the proposed strategy. Upon examining the aforementioned analysis, our conclusion is that the FCS-MPC strategy with a double closed loop, utilizing grey prediction and fuzzy dynamic weighting factors, has the capability to efficiently eliminate speed overshoot and enhance dynamic response. This approach leverages historical data to more accurately select the optimal voltage vector, thereby achieving an optimal allocation of multi-objective weight factors within the cost function. Additionally, it optimizes the switching times of the inverter to a certain extent and reduces the THD value of A-phase current, thereby enhancing the system's dynamic capabilities and resistance to interference. Therefore, the double closed loop FCS-MPC strategy based on grey prediction and fuzzy dynamic weighting factors offers significant advantages. However, it should be noted that this strategy slightly increases the computational burden. Consequently, future work will focus on minimizing this computational load while preserving the high-performance operation of the PMSM.

REFERENCES

Kouro, S., Perez, M.A., Rodriguez, J., Llor, A.M., and Young, H.A. (2015). Model Predictive Control MPC's Role in the Evolution of Power Electronics. *IEEE Industrial Electronics Magazine*, 9(4), 8-21.

Lim, C.S., Levi, E., Jones, M., Abd R.N., and Hew, W.P. (2014). FCS-MPC-Based Current Control of a Five-Phase Induction Motor and its Comparison with PI-PWM Control. *IEEE Transactions on Industrial Electronics*, 61(1), 149-163.

Li, T., Sun, X.D., Yang, Z.B., and Lei, G. (2024). Simplified two-step model predictive control with fast voltage vector search. *IEEE Transactions on Industrial Electronics*, Early Access.

Guo, Z., Liu, Q.Y., Chen, S.H., Hu, W.H., and Chen, Z. (2023). Two-Phase Model Predictive Direct Duty-Cycle Control for PMSM With Off-Line Lookup Table. *IEEE Transactions on Energy Conversion*, 38(4), 2796-2810.

Zhang, X.G., Bai, H.L., and Cheng, M. (2022). Improved model predictive current control with series structure for PMSM drives. *IEEE Transactions on Industrial Electronics*, 69(12), 12437-12446.

Lee, Y.S., Choo, K.M., Lee, C.H, An, C.G., Yi, J, and Won, C.Y. (2024). Common-mode voltage reduction method based on variable sampling frequency finite control set-model predictive control for PMSM drive systems. *Energies*, 17(6), 325-337.

Kusuma, E., Eswar, K.M.R., and Kumar, T.V. (2021). An effective predictive torque control scheme for PMSM drive without involvement of weighting factors. *IEEE J Emerg Selected Topics Power Electron*, 9(3), 2685-2697.

Hu, L., Lei, W.J., Li, R.X., and Gao, Y.C. (2023). A graphic weighting factor design method for finite control set model predictive control of power converters. *IEEE Journal of Emerging and Selected Topics in Power Electronics*, 11(2), 1661-1671.

Liu, X.C., Wang, J., Gao, X.N., Tian, W., Zhou ,L.B., and Kennel, R. (2022). Robust Predictive Speed Control of SPMSM Drives With Algebraically Designed Weighting Factors. *IEEE Transactions on Power Electronics*, 37(12), 14434-14446.

Wang, F.X., Li, J.X., Li, Z., Ke, D.L., Du, J.M., Garcia, C., and Rodriguez, J. (2022). Design of Model Predictive Control Weighting Factors for PMSM Using Gaussian Distribution-Based Particle Swarm Optimization. *IEEE Transactions on Industrial Electronics*, 69(11), 10935-10946.

Vazquez, S., Marino, D., Zafra, E., Peña, M.D.V., Rodríguez-Andina, J.J., Franquelo, L.G., and Manic, M. (2022). An Artificial Intelligence Approach for Real-Time Tuning of Weighting Factors in FCS-MPC for Power Converters. *IEEE Transactions on Industrial Electronics*, 69(12), 11987-11998.

Yao, C.X., Ma, G.T., Sun, Z.Y., Luo, J., Ren, G.Z., and Xu, S. (2024). Weighting Factors Optimization for FCS-MPC in PMSM Drives Using Aggregated Residual Network. *IEEE Transactions on Power Electronics*, 39(1), 1292-1307.

Huang, X., Guan, P., Pan, H., Liu, S., Du, G., Huang, X., and Wang, X. (2021). Research on grey predictive control of PMSM based on reduced-order luenberger observer. *Journal of Electrical Engineering & Technology*, 16(5), 2635–2646.

Karamanakos, P. and Geyer, T. (2020). Guidelines for the design of finite control set model predictive controllers. *IEEE Transactions on Power Electronics*, 35(7), 7434–7450.

Koiwa, K., Kuribayashi, T., Zanma, T., Liu, K.Z., and Wakaiki, M. (2019). Optimal current control for PMSM considering inverter output voltage limit: model predictive control and pulse-width modulation. *IET Electric Power Applications*, 13(12), 2044–2051.

Li, L., Xiao, J., Zhao, Y., Liu, K., Peng, X., Luan, H., and Li, K. (2020). Robust position anti-interference control for PMSM servo system with uncertain disturbance. *CES Transactions on Electrical Machines and Systems,* 4(2), 151–160. doi: 10.30941/CESTEMS.2020.00020.

Liang, D., Li, J., Qu, R., and Kong, W. (2018). Adaptive second-order sliding-mode observer for PMSM sensorless control considering VSI nonlinearity. *IEEE Transactions on Power Electronics,* 33(10), 8994–9004.

Liu, X., Zhou, L., Wang, J., Gao, X., Li, Z., and Zhang, Z. (2020). Robust predictive current control of permanent magnet synchronous motors with newly designed cost function. *IEEE Transactions on Power Electronics*, 35(10), 10778–10788.

Novak, M., Xie, H., Dragicevic, T., Wang, F., Rodriguez, J., and Blaabjerg, F. (2021). Optimal cost function parameter design in predictive torque control (PTC) using artificial neural networks (ANN). *IEEE Transactions on Industrial Electronics*, 68(8), 7309–7319.

Siami, M., Arab Khaburi, D., and Rodriguez, J. (2018). Simplified finite control set-model predictive control for matrix converter-fed PMSM drives. *IEEE Transactions on Power Electronics,* 33(3), 2438–2446.

Wang, Z., Yang, M., Gao, L., Wang, Z., Zhang, G., Wang, H., and Gu, X. (2020). Deadbeat predictive current control of permanent magnet synchronous motor based on variable step-size adaline neural network parameter identification. *IET Electric Power Applications*, 14(11), 2007–2015.

Xuan, J., Wang, X., Lu, D., and Wang, L. (2017). Research on the safety assessment of the brushless DC motor based on the gray model. *Advances in Mechanical Engineering,* 9(3), 436-449.

Yang, J., Liu, Y., and Yan, R. (2021). A comparison of finite control set and continuous control set model predictive control schemes for model parameter mismatch in three phase APF. *Frontiers in Energy Research*, 9(5), 465-476.

Yu, B., Song, W., Yang, K., Guo, Y., and Saeed, M.S.R. (2022). A computationally efficient finite control set model predictive control for multiphase PMSM drives. *IEEE Transactions on Industrial Electronics*, 69(12), 12066–12076.

Zhang, X. and Hou, B. (2018). Double vectors model predictive torque control without weighting factor based on voltage tracking error. *IEEE Transactions on Power Electronics*, 33(3), 2368–2380.